Supporting information

Synthesis of Double-Bridged Cofacial Nickel Porphyrin Dimers with 2,2'-Bipyridyl Pillars and Their Restricted Coordination Space

Akiharu Satake[1) 2)]*, *Yuta Katagami*[1)], *Yuki Odaka*[1)], *Yusuke Kuramochi*[1) 2)], *Shohei Harada*[1)], *Takaya Kouchi*[1)], *Hajime Kamebuchi*[1) 3)], *and Makoto Tadokoro*[1) 3)]

1) Graduate School of Science, Tokyo University of Science, 1-3 Kagurazaka, Shinjuku-ku, Tokyo 162-8601 (Japan)

2) Department of Chemistry, Faculty of Science Division II, Tokyo University of Science.

3) Department of Chemistry, Faculty of Science Division I, Tokyo University of Science.

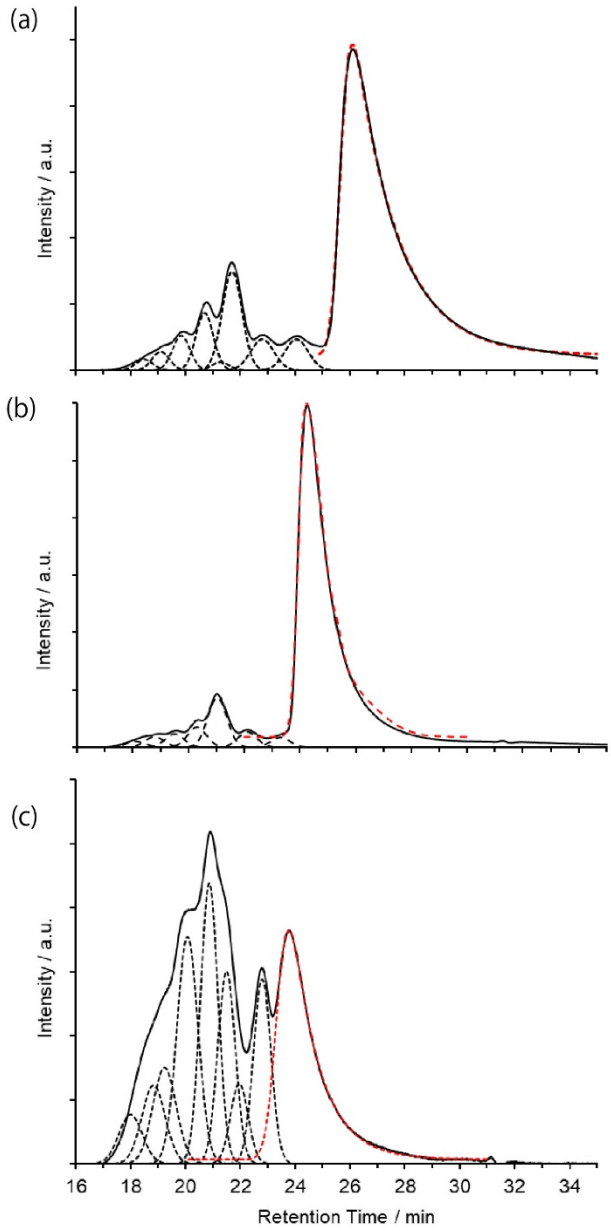

Figure S1. GPC charts (solid lines) of reaction mixtures from (a) $\mathbf{1}_{\mathbf{Me}}$, (b) $\mathbf{1}_{\mathbf{Bu}}$, and (c) $\mathbf{1}_{\mathbf{Oc}}$; GPC conditions: Tosoh G2500H$_{HR}$×2 + G2000H$_{HR}$×1 (columns), pyridine (eluent), 1.0 mL/min (flow rate), monitored at 536 nm in (a) and (b), and 563 nm in (c). Curve-fitting analyses show dotted lines, in which the red lines correspond to the cyclic porphyrin dimers.

Table S1. Crystal data and structure refinement

Compound	$\mathbf{2_{Oc}}$	$\mathbf{2_{Bu}}$	$\mathbf{2_{Bu}}$**-(allylPd)$_2$**
Temperature (K)	173	173	173
Crystal system	*Triclinic*	*Monoclinic*	*Monoclinic*
Space group	*P*-1(#2)	*C*2/c(#15)	$P2_1/n$(#14)
a (Å)	13.725(8)	20.464(8)	16.4955(5)
b (Å)	14.935(8)	21.756(8)	16.5823(6)
c (Å)	15.352(9)	27.647(10)	29.2556(9)
α (deg)	92.577(7)	90	90
β (deg)	109.984(6)	98.453(4)	105.4930(10)
γ (deg)	99.780(7)	90	90
V (Å^3)	2896(3)	12175(8)	7711.6(4)
Z	1	4	2
$D_{calc.}$ (mg/m^3)	1.225	1.259	1.377
F_{000}	1132	4769	3246
Theta range for data collection (< 2*θ*)	3.220 to 55.118°	2.748 to 50.052°	4.912 to 50.052°
Reflections collected	15010	26227	83582
Independent reflections	12036 [R(int) = 0.0311]	10653 [R(int) = 0.0743]	13588 [R(int) = 0.0744]
Final *R* indices [I>2*θ*(I)]	R_1= 0.0729, wR_2 = 0.1988	R_1 = 0.0799, wR_2 = 0.2274	R_1 = 0.0543, wR_2 = 0.1393
R indices (all data)	R_1 = 0.1216, wR_2 = 0.2156	R_1 = 0.1471, wR_2 = 0.2820	R_1 = 0.0697, wR_2 = 0.1546
Goodness-of-fit	1.105	1.008	1.031

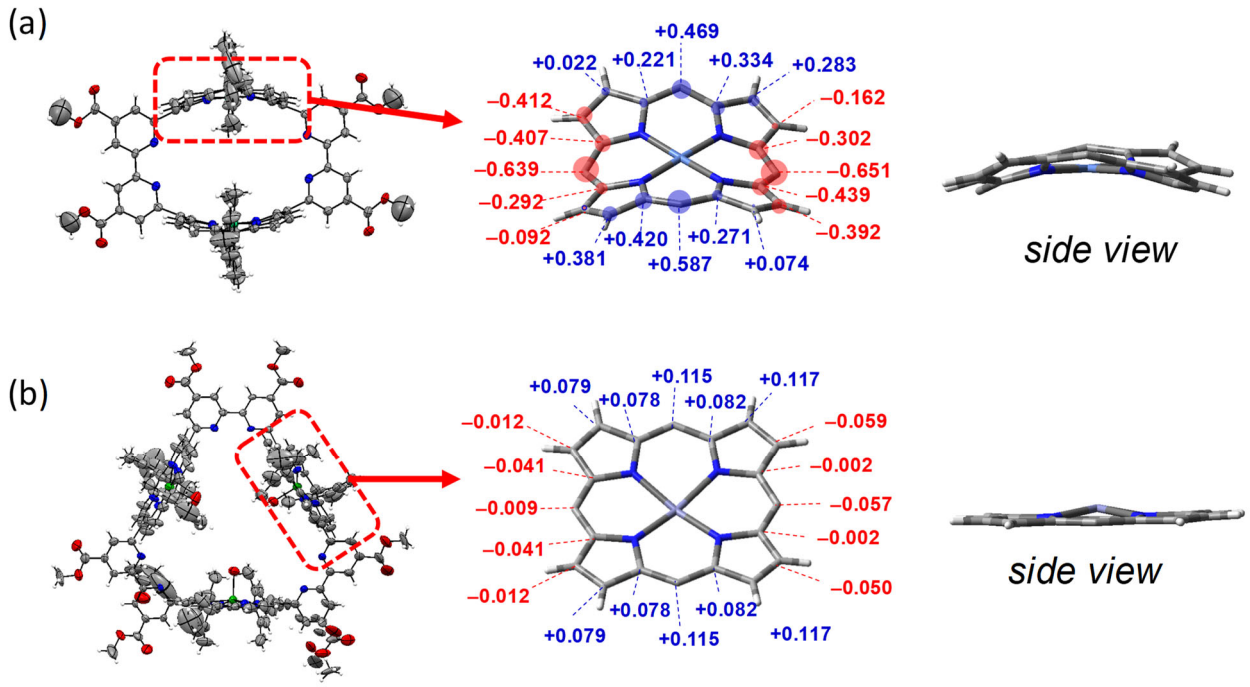

Figure S2. Crystal structures of (a) cyclic dimer of Ni(II) porphyrin $\mathbf{2}_{\mathbf{Oc}}$ and (b) cyclic trimer of Zn(II) porphyrin **Zn-3**$_{\mathbf{Me}}$. ORTEP views (left), the deviations of selected atoms (in Å) from the 4N mean planes (center), and side views of the porphyrin parts (right).

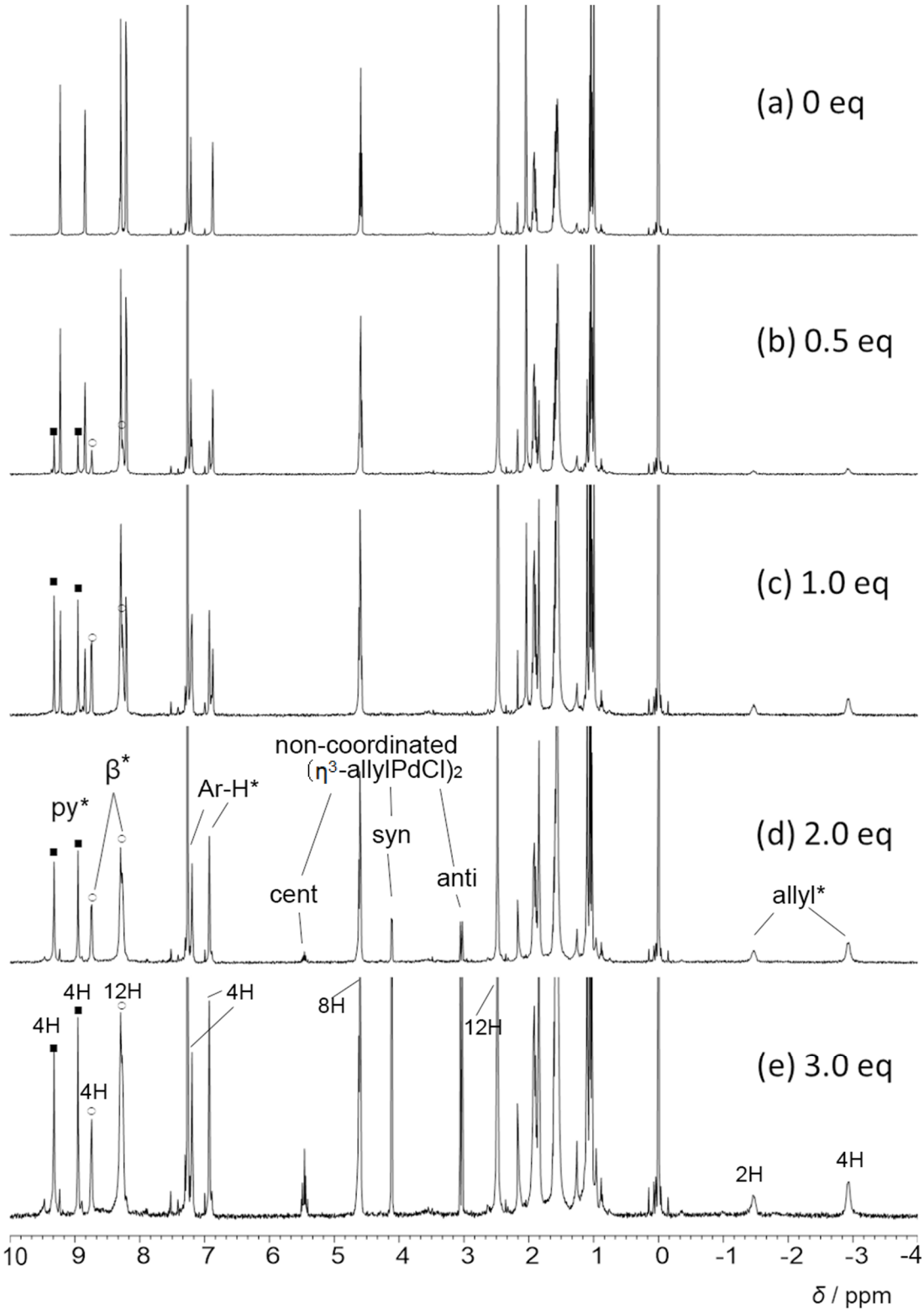

Figure S3. ^{1}H NMR (400 MHz) titration of cationic η^3–allylpalladium terafluoroborate complexes into $\mathbf{2_{Bu}}$ in $CDCl_3$ at 24 °C. (Enlargement between 10.0 and 6.5 ppm. See Figure 6.) From the top to the bottom: 0, 0.5, 1.0, 2.0, and 3.0 equiv. of the palladium species.

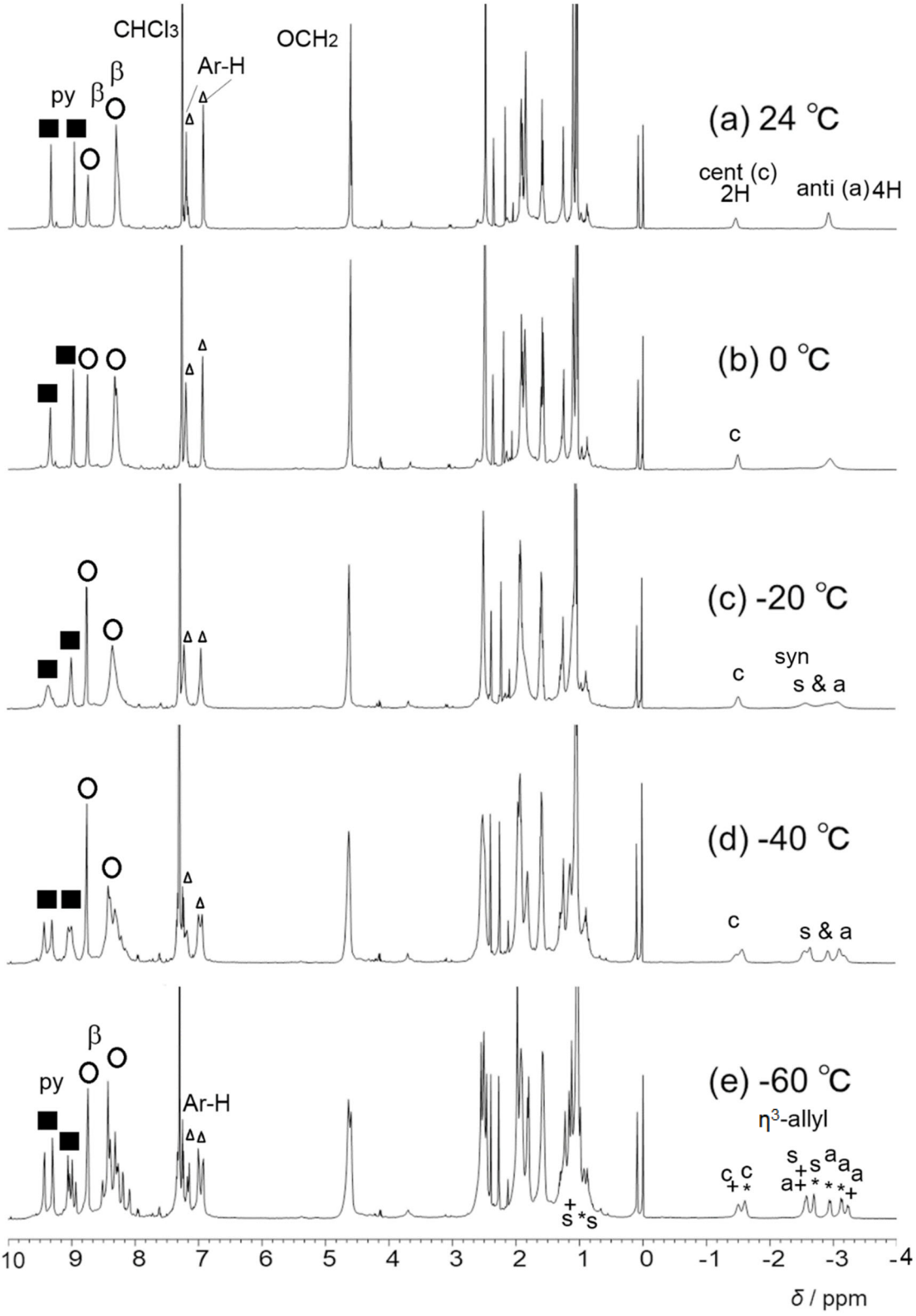

Figure S4. VT-^{1}H NMR spectra (400 MHz, $CDCl_3$) of a 2:1 mixture of cationic η^3–allylpalladium complexes and $\mathbf{2_{Bu}}$. (a) 24 °C, (b) 0 °C, (c) –20 °C, (d) –40 °C, (e) –60 °C

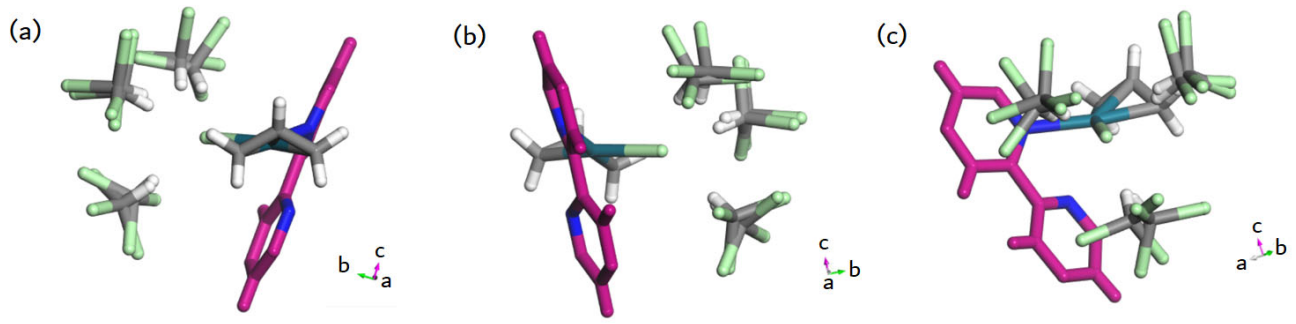

Figure S5. A η^3-allyl palladium chloride moiety in the molecular structure of **2_{Bu}-(allylPd)$_2$** obtained by the XRD analysis. Purple colored atoms correspond to the 2,2'-bipyridyl part. The η^3-allyl palladium chloride and $CHCl_3$ molecules are shown as light green (chlorine), green (palladium), blue (nitrogen), gray (carbon), and white (hydrogen atoms). (a) a front view of the η^3-allyl group, (b) (c) from other angles.

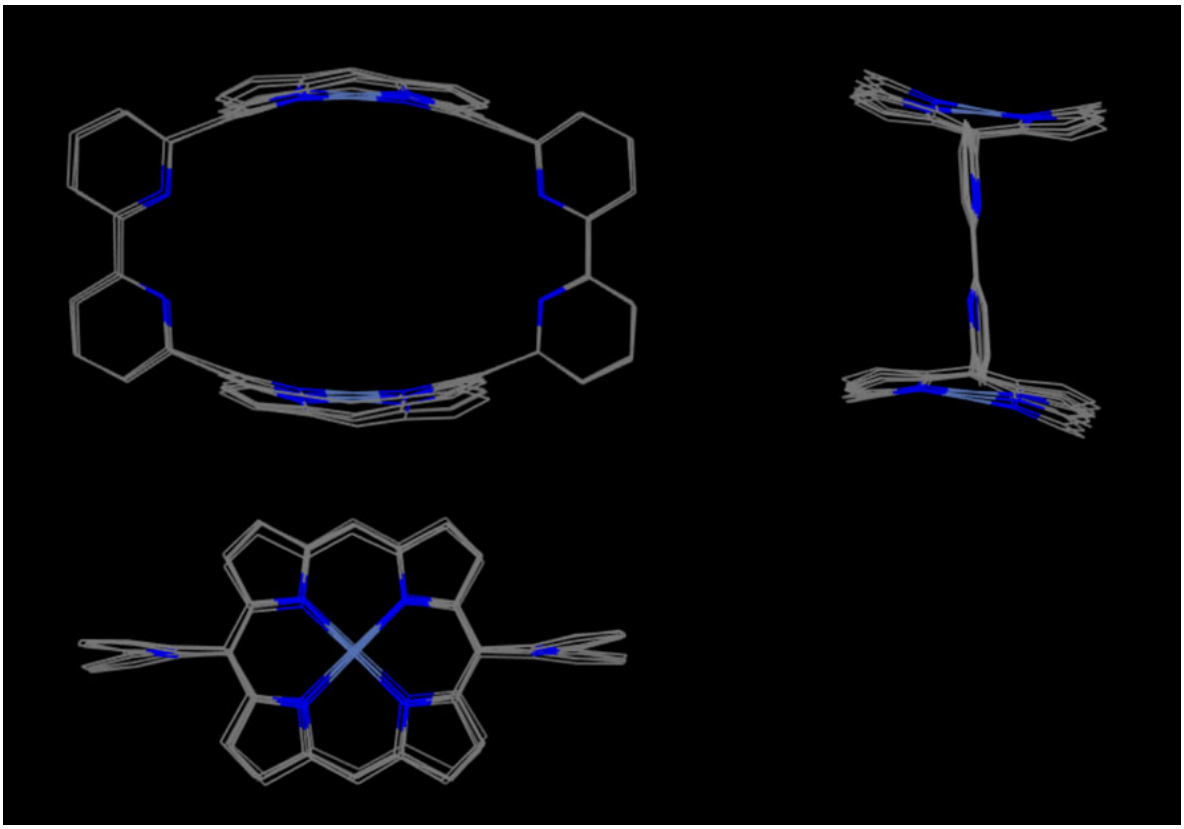

Figure S6. Macrocyclic frameworks composed of two porphyrin and two bipyridyl groups in **2_{Oc}**, **2_{Bu}**, **2_{Bu}-(allylPd)$_2$** (overlaid).

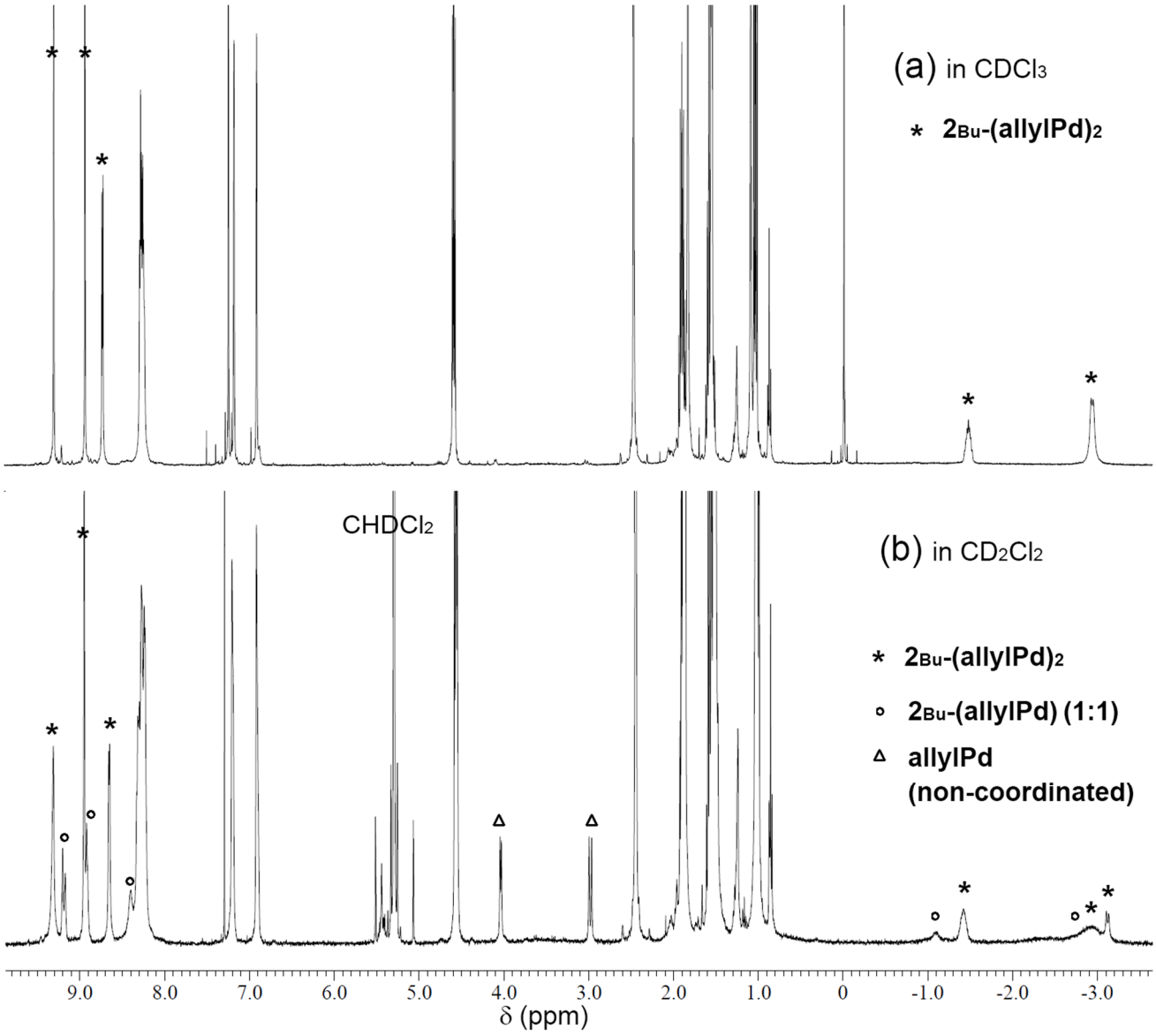

Figure S7. ^{1}H NMR spectra (400 MHz, at rt) of **2_{Bu}-(allylPd)$_2$** (purified by recrystallization) in (a) $CDCl_3$ and (b) CD_2Cl_2. In (b), **2_{Bu}-(allylPd)$_2$** : **2_{Bu}-(allylPd)** (1:1 complex) = 71:29.

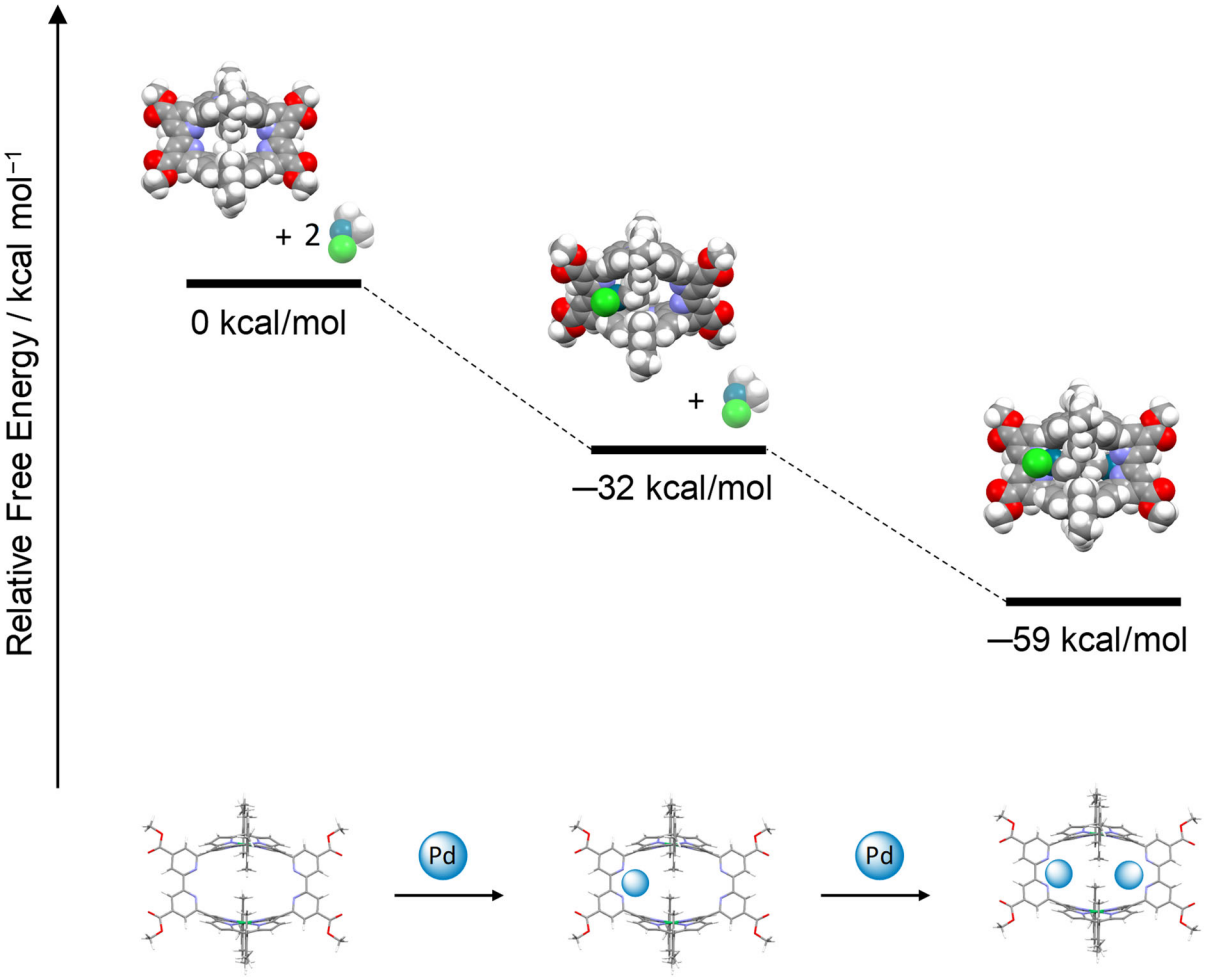

Figure S8. Relative Gibbs free energy profiles of $\mathbf{2^{Me}}$ and the η^3–allylpalladium complexes. The structures were optimized at the B3LYP/LANL2DZ (Ni, Pd)/6-31G(d) (H, N, C, O, Cl) level in vacuo.

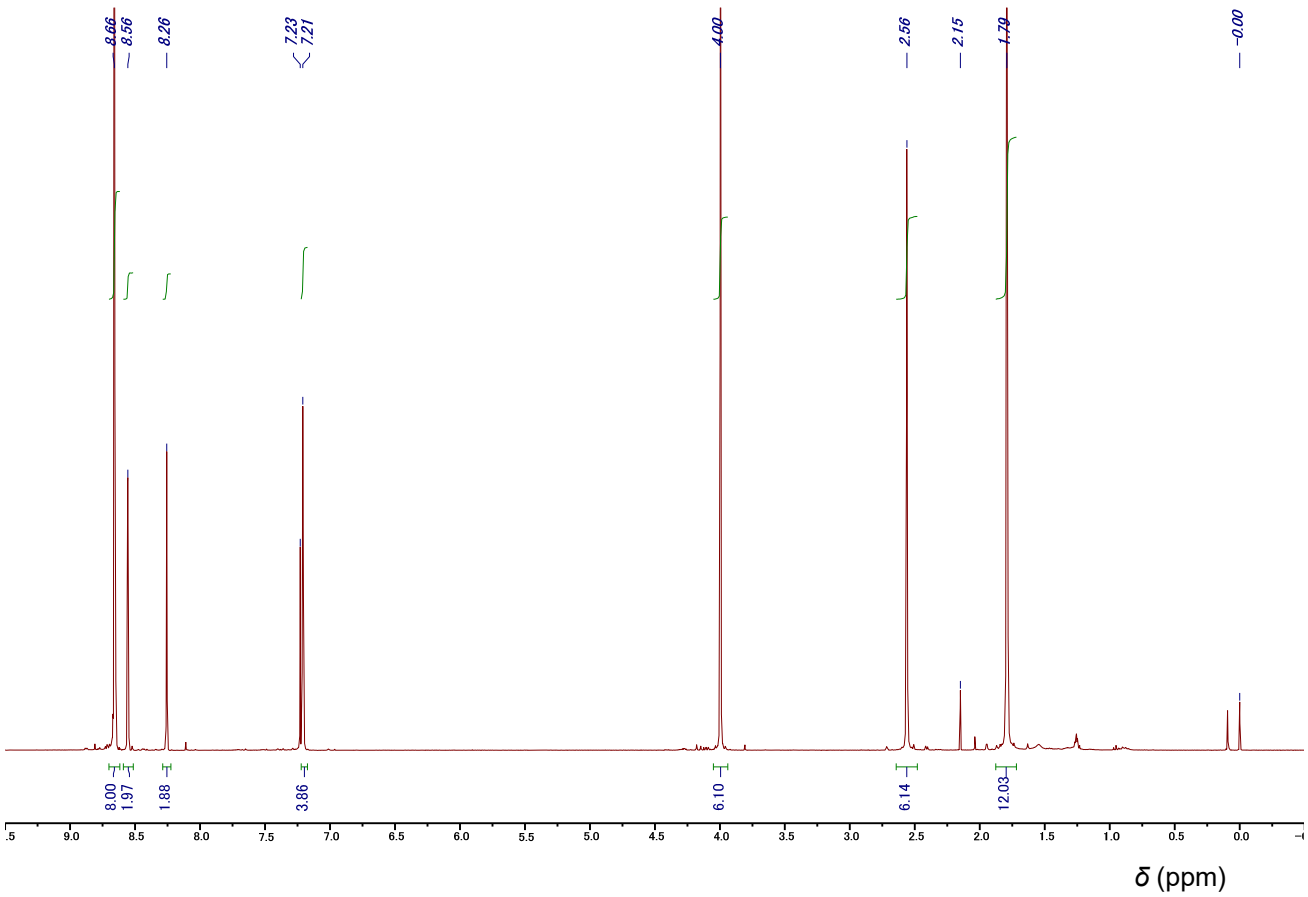

Figure S9. ^{1}H NMR spectrum (400 MHz, $CDCl_3$) of $\mathbf{1_{Me}}$.

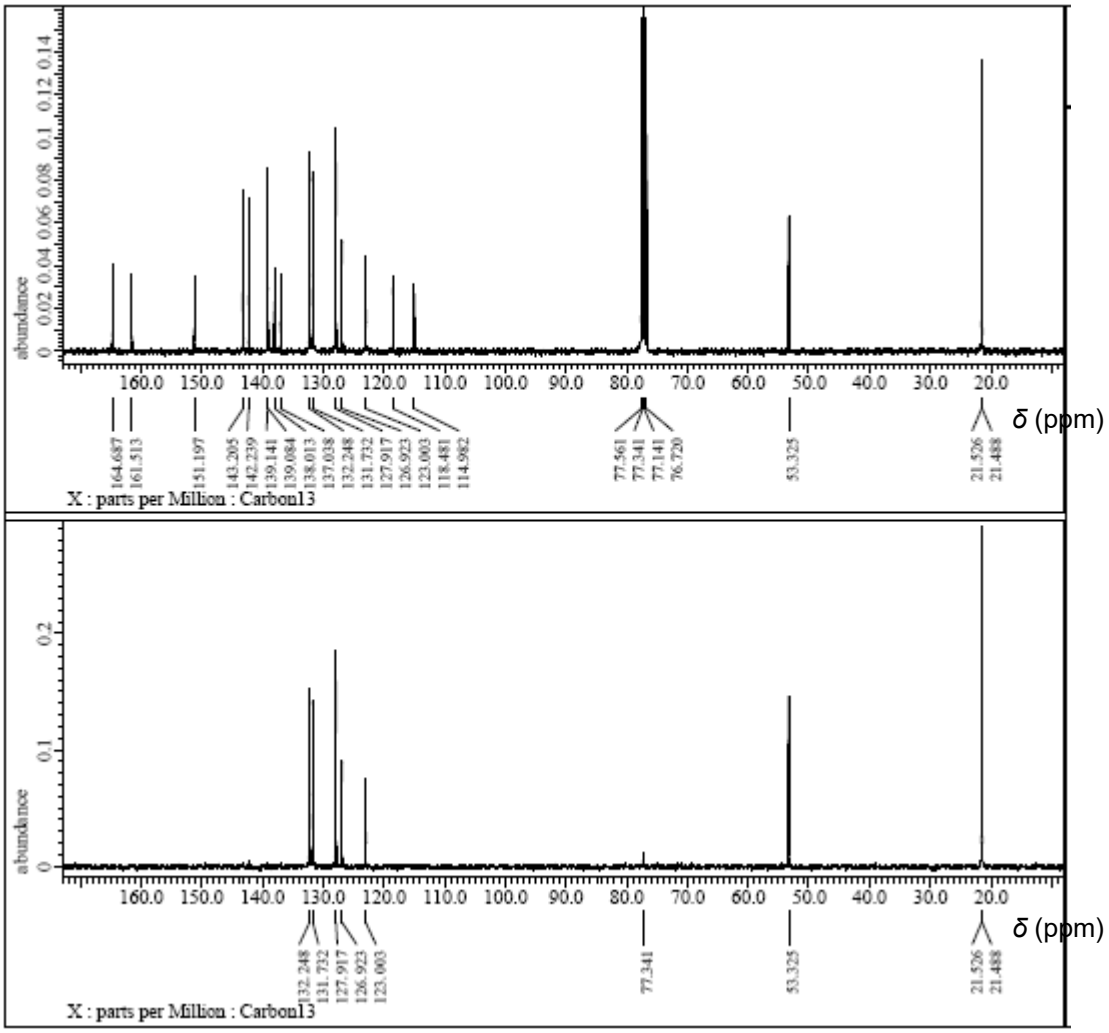

Figure S10. ^{13}C NMR spectrum (upper) and DEPT135 (lower) of $\mathbf{1_{Me}}$ (100 MHz, $CDCl_3$).

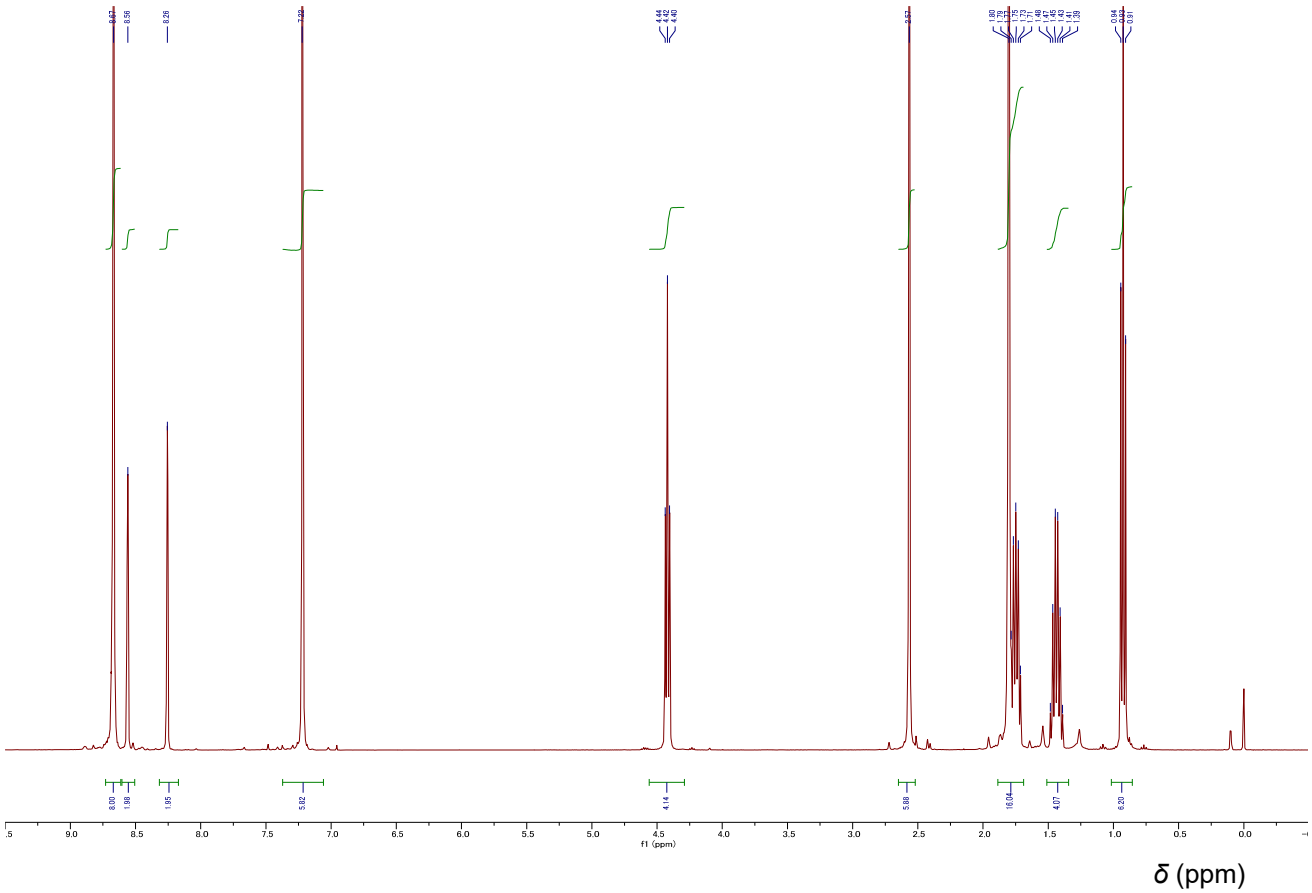

Figure S11. ^{1}H NMR spectrum (400 MHz, $CDCl_3$) of $\mathbf{1_{Bu.}}$

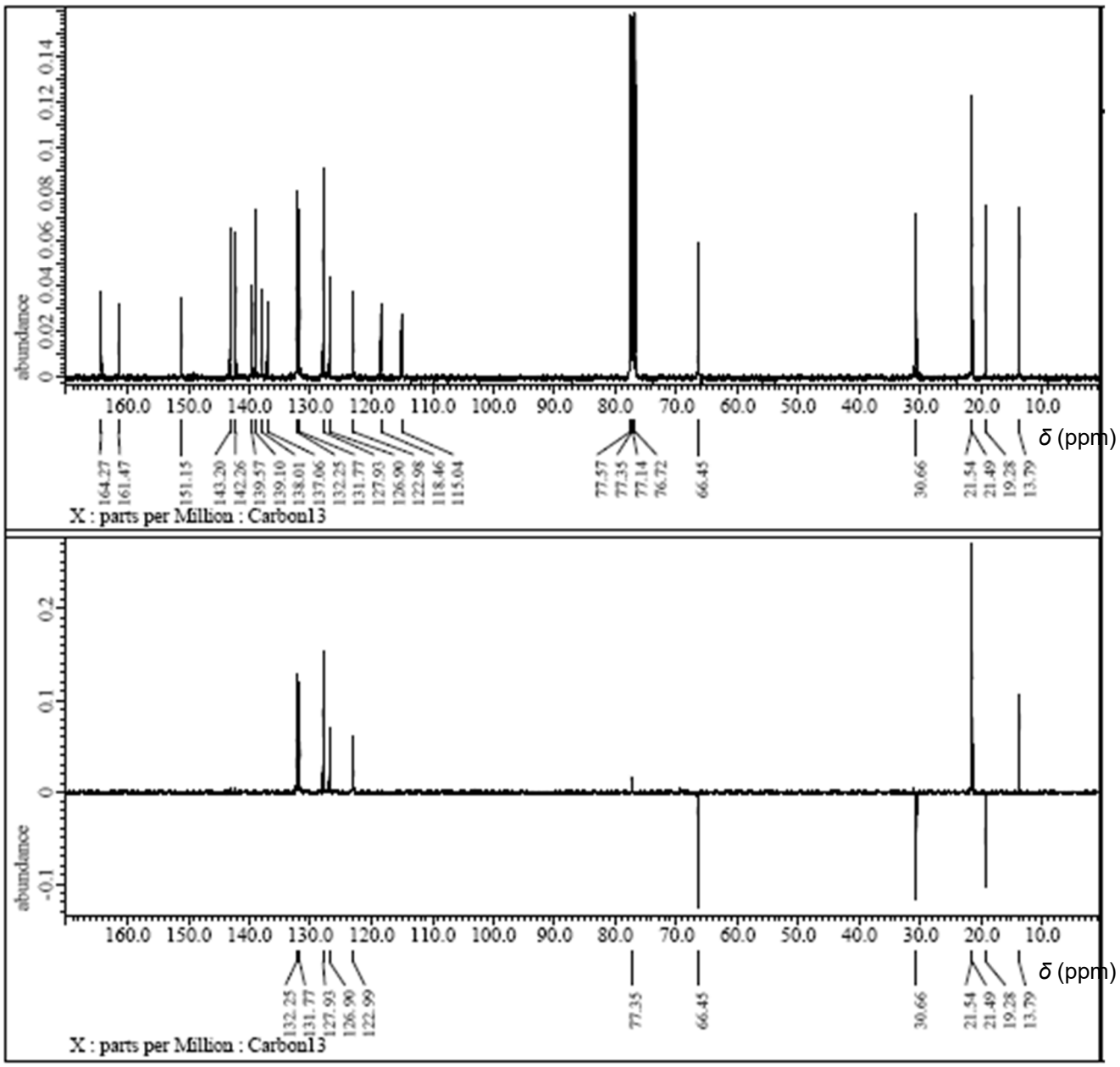

Figure S12. (upper) ^{13}C NMR (100 MHz, $CDCl_3$) of $\mathbf{1_{Bu}}$. (lower) DEPT135.

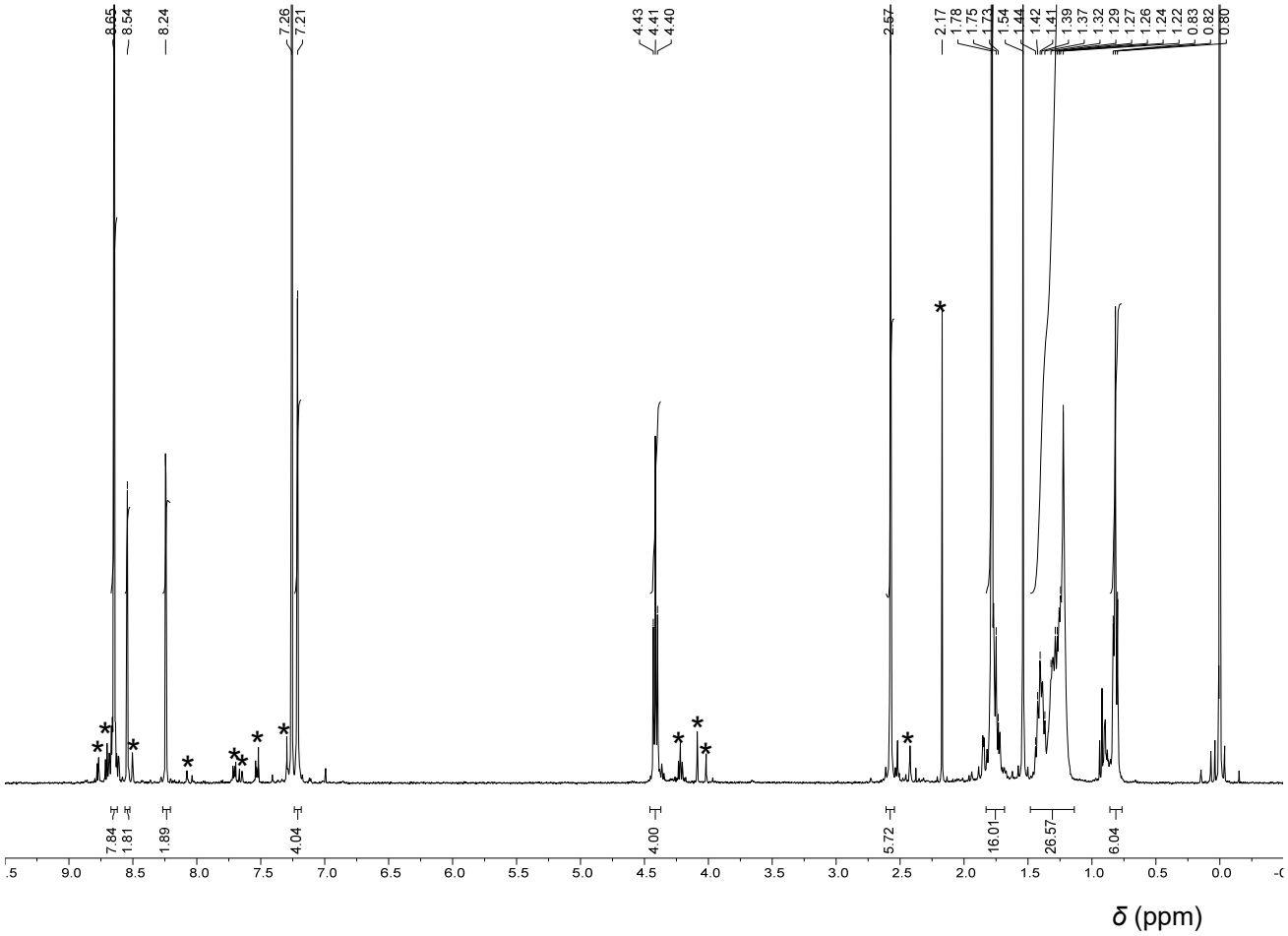

Figure S13. ^{1}H NMR (500 MHz, $CDCl_3$) of $\mathbf{1_{Oc}}$. The peaks marked as (*) indicate impurities which can be removed after the homo coupling reaction.

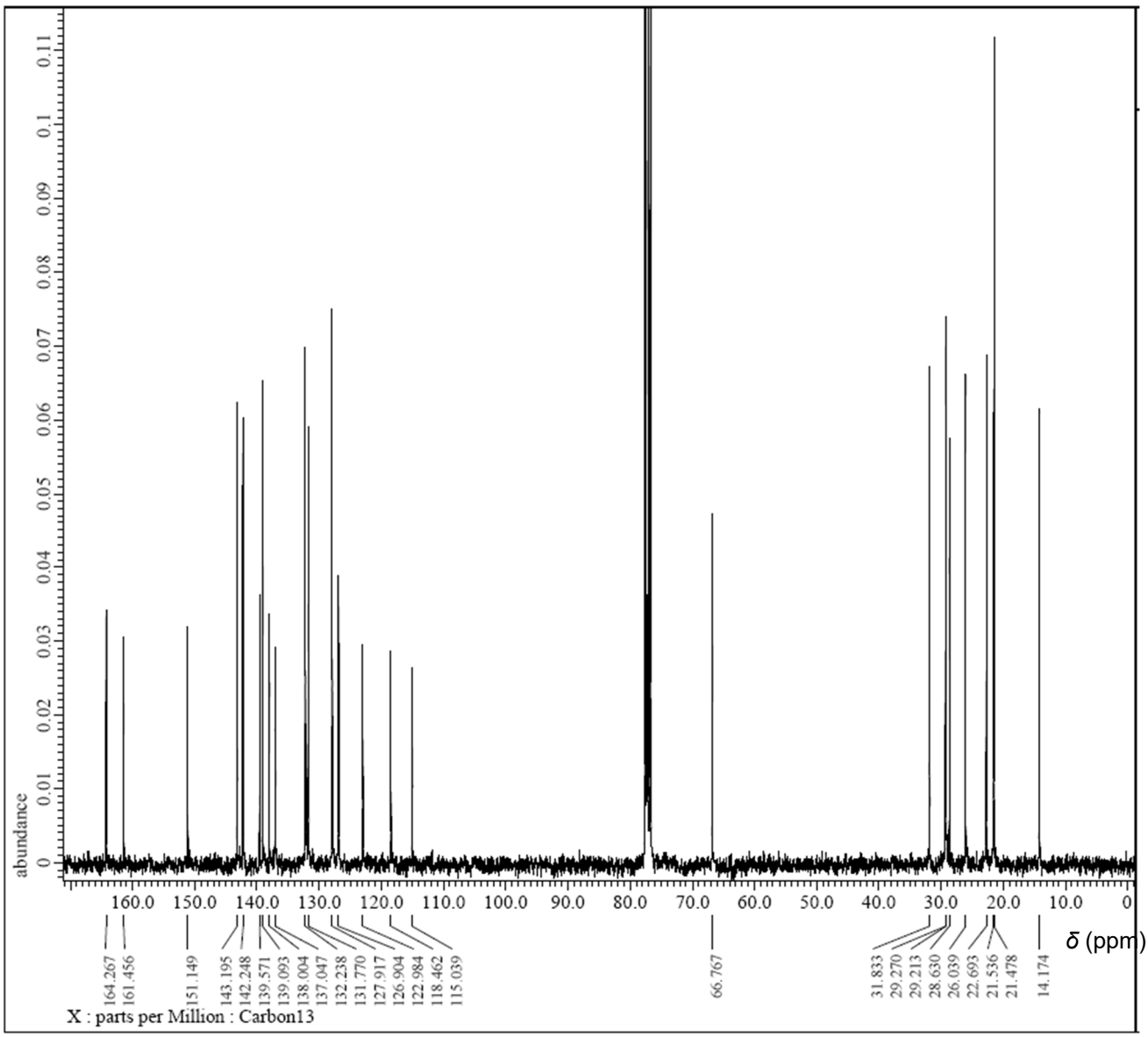

Figure S14. ^{13}C NMR (125 MHz, $CDCl_3$) of $\mathbf{1_{Oc}}$.

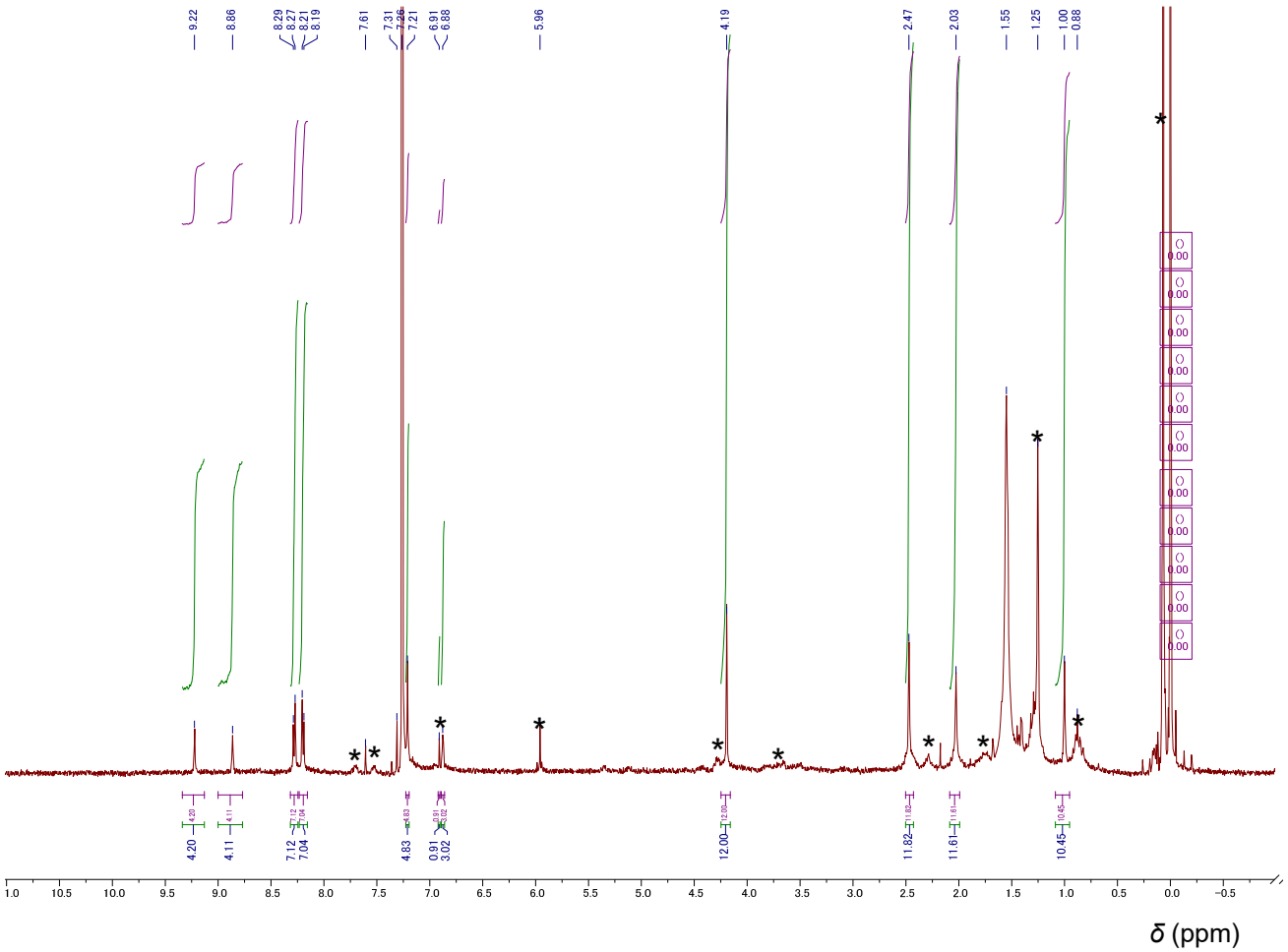

Figure S15. ^{1}H NMR (300 MHz, $CDCl_3$) of $\mathbf{2_{Me}}$. Because compound $\mathbf{2_{Me}}$ tended to be self-aggregated, the solubility was very low in any solvent. In particular, purified $\mathbf{2_{Me}}$ was difficult to be measured by ^{1}H NMR. The above ^{1}H NMR spectrum was collected as a roughly purified sample. The peaks marked as (*) correspond to impurities including other linear oligomers.

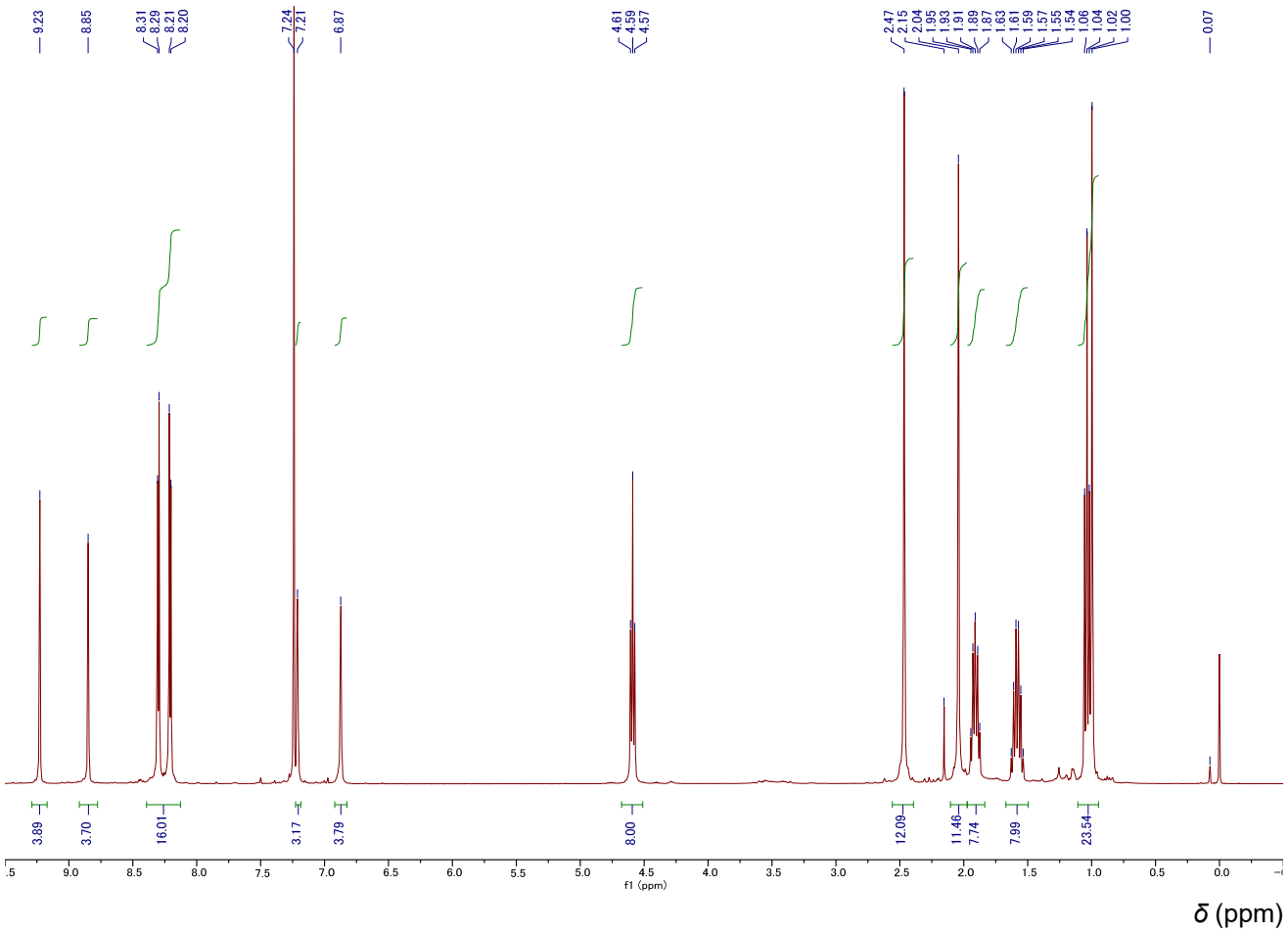

Figure S16. ^{1}H NMR (400 MHz, $CDCl_3$) of $\mathbf{2_{Bu}}$.

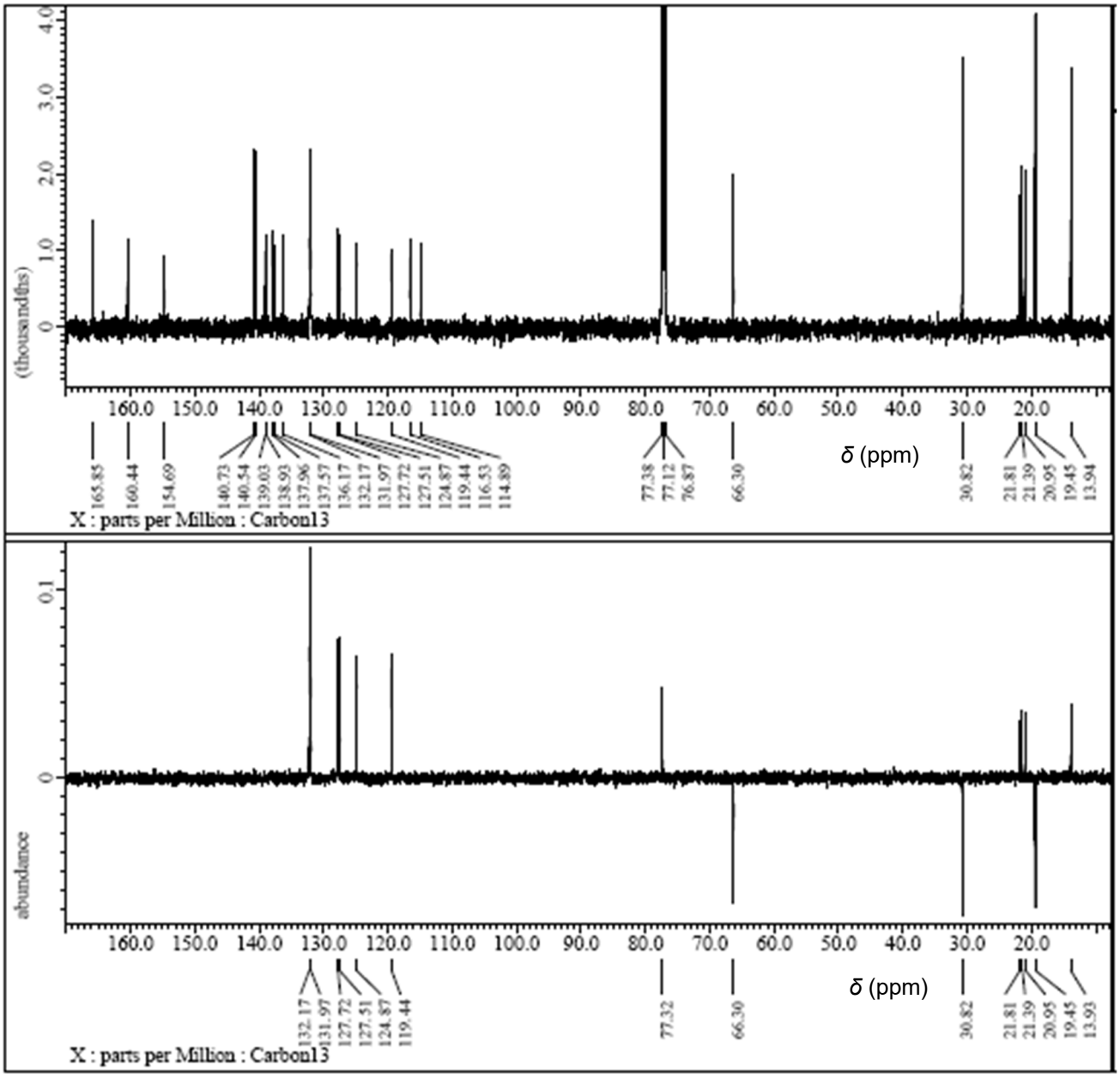

Figure S17. (upper) ^{13}C NMR (100 MHz, $CDCl_3$) of $\mathbf{2_{Bu}}$. (lower) DEPT135.

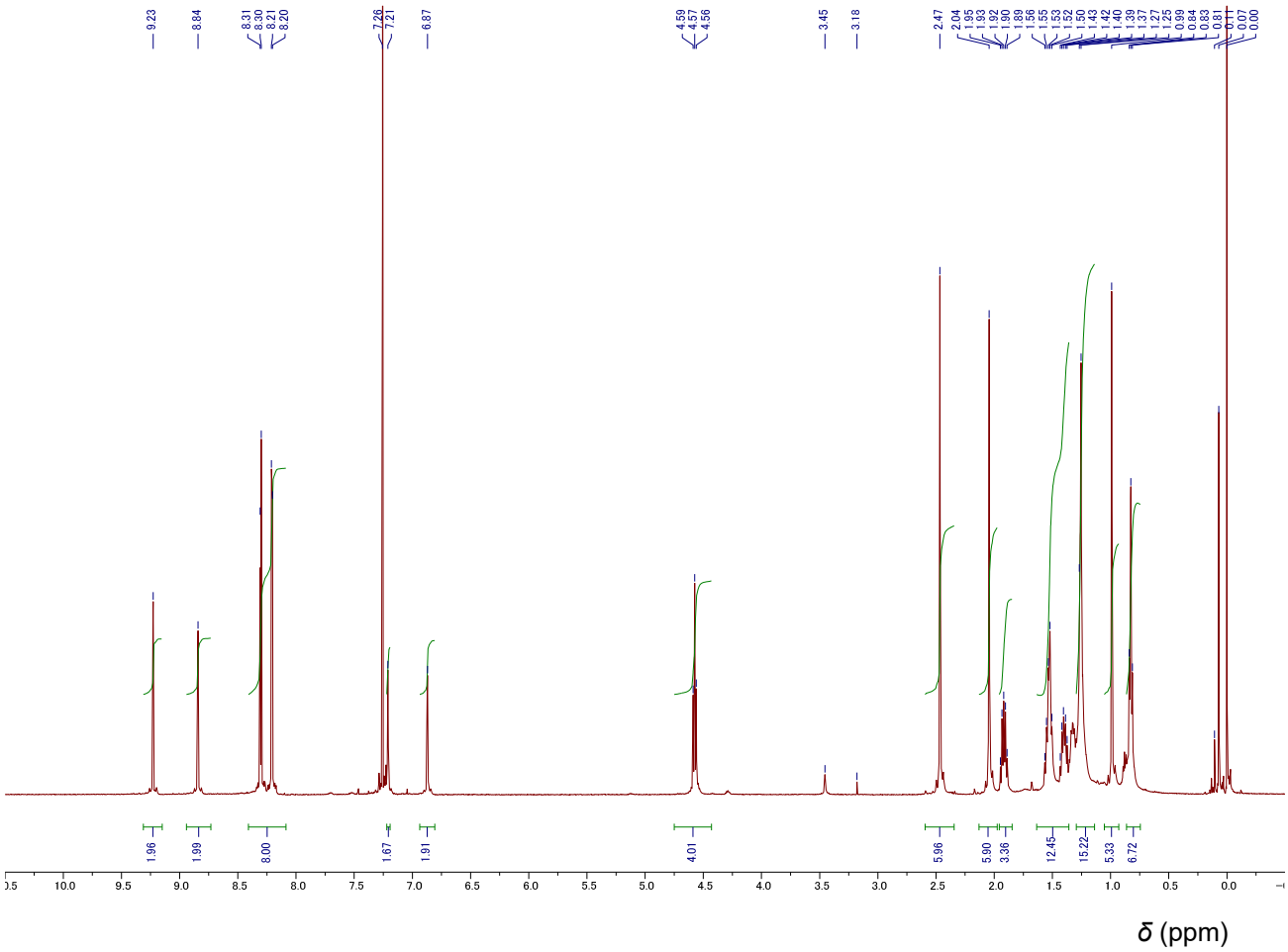

Figure S18. ^{1}H NMR (500 MHz, $CDCl_3$) of $\mathbf{2_{Oc}}$.

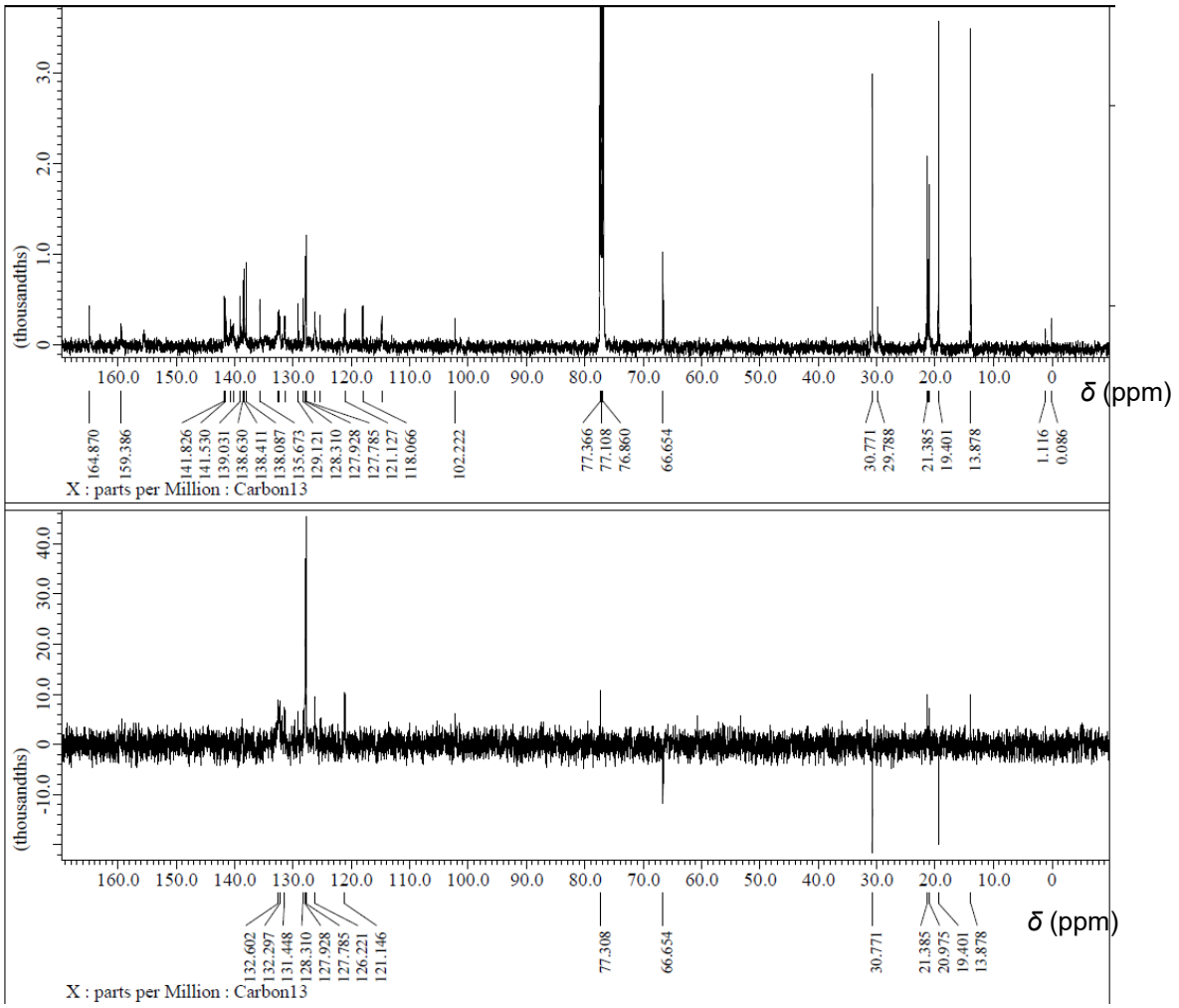

Figure S19. (upper) ^{13}C NMR (125 MHz, $CDCl_3$) of **2_{Bu}-(allylPd)$_2$** at 23 °C. (lower) DEPT135.

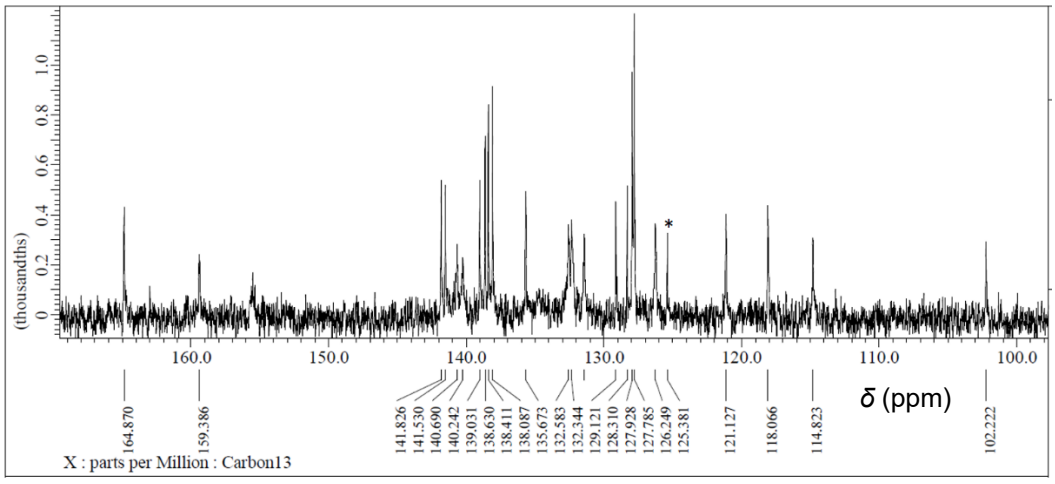

Figure S20. ^{13}C NMR (125 MHz, $CDCl_3$) of **2_{Bu}-(allylPd)$_2$** at 23 °C. (same as **Figure S19** (upper) expanded).

*: impurity.

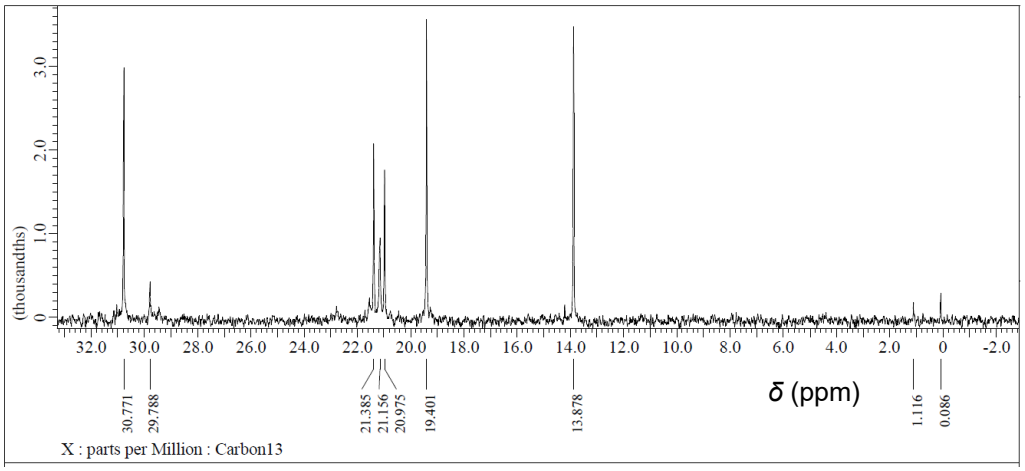

Figure S20. continued.

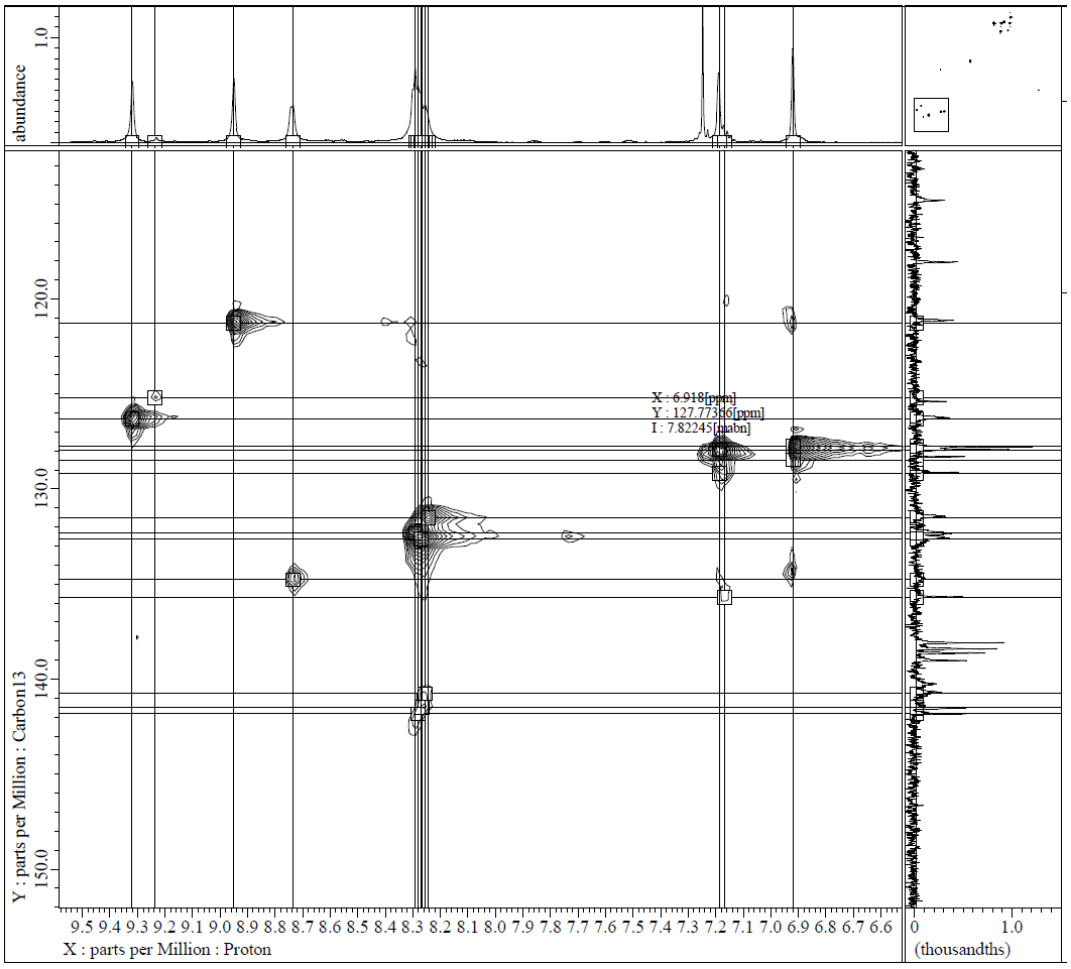

Figure S21. HSQC spectrum of **2_{Bu}-(allylPd)$_2$** in $CDCl_3$ at 23 °C.

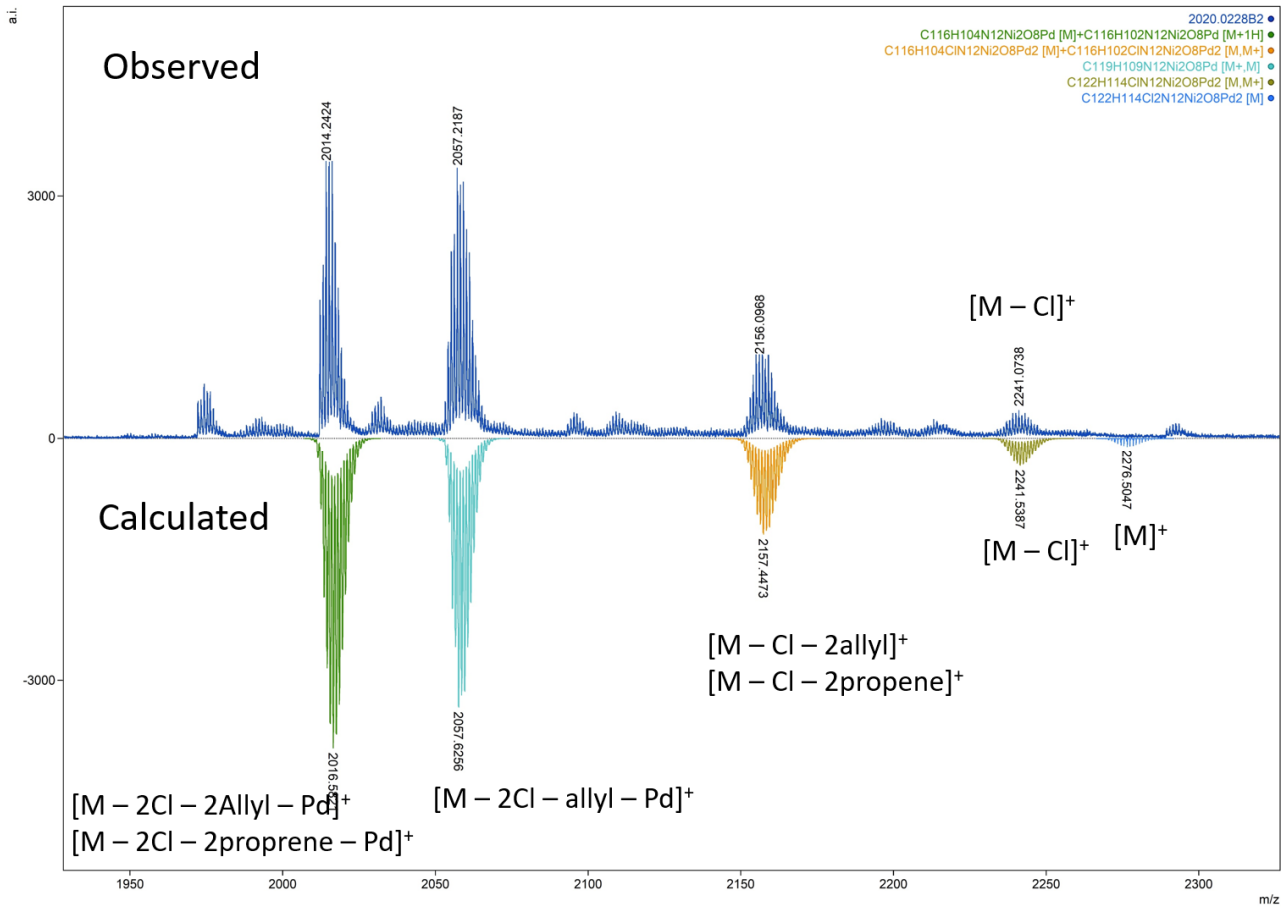

Figure S22. ESI-MS spectrum of $\mathbf{2_{Bu}\text{-}(allylPd)_2}$. (upward) observed. (downward) calculated.